Hidden Reservoir of Photoactive Electrons in $LiNbO_3$ Crystals

F. Luedtke,[1,*] K. Buse,[2,3] and B. Sturman[4]

[1]*Institute of Physics, University of Bonn, Wegelerstrasse 8, 53115 Bonn, Germany*
[2]*Department of Microsystems Engineering, University of Freiburg, 79110 Freiburg, Germany*
[3]*Fraunhofer Institute of Physical Measurement Techniques, Heidenhofstrasse 8, 79110 Freiburg, Germany*
[4]*Institute of Automation and Electrometry of RAS, Koptyug Avenue 1, 630090 Novosibirsk, Russia*

(Received 23 December 2011; published 13 July 2012)

We show that a continuous-wave (cw) pump beam at a wavelength of 532 nm produces substantial light-induced (LI) absorption in the visible range in initially transparent undoped $LiNbO_3$ crystals. The LI absorption coefficient stays linear in the pump intensity I_p up to $I_p^{max} = 48$ kW/cm^2. Together with other features including long-term stretched-exponential relaxation of the LI absorption, it indicates that the present concept of LI electron processes in this important optical material must be revised: the amount of photoactive electrons increases already within the cw intensity range. A quantitative model is proposed that explains the experimental data and employs two-step excitations from filled localized states near the valence band via intermediate deep centers into the conduction band. The introduced localized states serve as a hidden reservoir of electrons.

DOI: 10.1103/PhysRevLett.109.026603 PACS numbers: 72.20.Jv, 42.70.Nq, 78.20.Bh

Lithium niobate is a wide band-gap ($\simeq 3.8$ eV) optical material which is of prime importance for numerous applications, e.g., for electro-optic modulation and frequency conversion [1]. The advent of domain patterning and microresonators increases the usability of this material [2,3], enhancing the role of its optical properties. Light-induced (LI) charge transport, dominated typically by the bulk photovoltaic effect [4,5] and leading to large electric fields and strong index changes, is of relevance for practically any application. This is why the efforts to understand and control the charge-transport properties have persisted for more than three decades [6–8].

It is known that, for congruent crystals doped with Fe, Cu, and other transition metals, the charge transport at sufficiently low continuous wave (cw) intensities ($I \lesssim 10^4$ W/cm^2) is due to LI transitions of electrons from deep traps to the conduction band (CB) [6,8]. For larger intensities, occupation of numerous ($\sim 10^{20}$ cm^{-3}) intermediate levels near the CB, attributed to the intrinsic Nb_{Li} defects, becomes important [6,9–12]. The total amount of photoactive electrons, which is controlled by doping and thermal treatments (reduction and oxidization), remains constant here: LI transitions lead only to redistribution of electrons between deep and intermediate levels and the CB. This is believed to be valid for undoped crystals with remnant impurity concentrations $\sim 10^{15}$ cm^{-3}.

According to the present concept, the valence band (VB) is involved in the LI charge transport either for UV illumination [13] or at high intensities [14–16] via two-photon pulse excitation at $I_{peak} \gg 1$ MW/cm^2. The LI absorption coefficient α_{li} is quadratic in I_{peak} in the last case, and the cross sections of the relevant excitation processes are quantified [16,17]. Occupation of the Nb_{Li} levels, which accompanies the CB excitation in any case, manifests itself in a characteristic long-term stretched-exponential relaxation of α_{li} [10,14,15].

In this Letter, we show experimentally that initially transparent undoped $LiNbO_3$ crystals become substantially more absorbing under cw optical pump illumination already when the two-photon excitation is negligible. Moreover, the LI absorption coefficient α_{li} grows linearly in the pump intensity I_p. These features indicate that the present concept of charge transport in $LiNbO_3$ crystals must be revised. A microscopic model explaining the observations by electron excitation from localized levels near the VB is proposed with far reaching consequences for the understanding and application of these crystals.

We employ a standard collinear pump-probe setup [7]: the pump beam from a frequency-doubled Nd:YAG laser with an output power of 5 W at $\lambda_p = 532$ nm induces the absorption changes. These changes are probed by low-intensity light beams from diode and Argon-ion lasers at $\lambda^* = 785$ and 488 nm. The pump and probe beams are focused independently and superimposed with a beam splitter such that the focal regions are placed in the middle of the sample. The probe beams are focused tighter than the pump beam: the ratio of $1/e^2$ beam radii is $r^*/r_p \simeq 0.6$. The maximum value of I_p is 48 kW/cm^2, and the depth of the focus of the probe beam, i.e., the effective interaction length, is $l^* \simeq 3$ mm.

The samples used are z cuts of congruent undoped lithium niobate of dimensions $11 \times 11 \times 7$ mm^3 supplied by Crystal Technology, Inc. The crystals have not undergone any kind of pretreatment. Their low-intensity light absorption coefficient α at λ_p and λ^* is smaller than the detection limit of $\alpha \approx 10^{-2}$ cm^{-1} of our absorption spectrometer. The samples are illuminated through the z faces

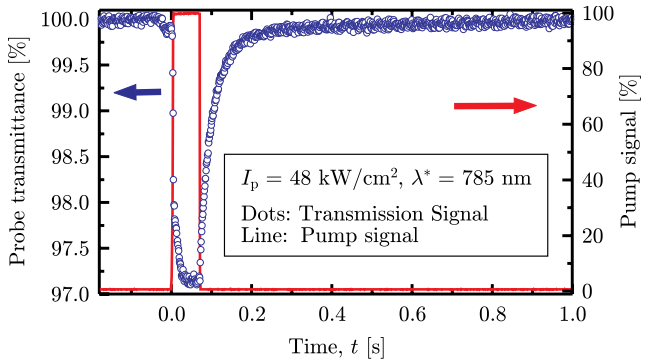

FIG. 1 (color online). Temporal evolution of the probe-beam transmittance at $\lambda^* = 785$ nm (open circles) upon switching the pump beam on and off (solid line).

such that the light beams are ordinarily polarized, and the photorefractive optical damage is suppressed.

The pump beam is switched on and off by a fast electromechanical shutter (switching time <100 μs). A silicon photodetector is used to monitor the resulting time-dependent probe signal behind the sample. Two identical digital oscilloscopes allow us to combine a high time resolution with a long measurement interval reaching several seconds. In order to improve the signal-to-noise ratio, we average the transmission signal over many (≥ 30) measurements; in this way, transmission changes well below 0.5% are reliably detected. Also, we change the sample position while keeping fixed the other parameters to verify reproducibility of the measurements.

Figure 1 shows a representative transmission signal upon switching the pump beam on and off. With the pump on ($t = 0$), the transmittance of the probe beam drops rapidly to $\simeq 97\%$ of the initial value. After switching off the pump ($t \simeq 0.07$ s), the transmittance relaxes relatively slowly to its initial value. Minimizing the exposure time (see Fig. 1) reduces heating of the sample.

The LI absorption coefficient α_{li} is calculated as $\alpha_{li} = \ln[1/T^*(t)]/l^*$, where T^* is the probe-beam transmittance normalized to its initial value with no pump beam present. In this way, we investigate the steady-state value of α_{li} versus the pump intensity I_p and the decay of α_{li} after switching the pump beam off.

Figures 2(a) and 2(b) show the steady-state values of α_{li} versus the pump intensity for $\lambda^* = 785$ and 488 nm. In both cases, the dependence $\alpha_{li}(I_p)$ is linear. Furthermore, the values of α_{li}^{785} are noticeably larger than those for α_{li}^{488}. At the lowest pump intensities, the values of $\alpha_{li}^{488}(I_p)$ are too small to be reliably measured.

The open circles in Figs. 3(a) and 3(b) show the experimental dependences $\alpha_{li}^{785}(t)$ and $\alpha_{li}^{488}(t)$ for different values of the pump intensity and more than three decades of the relaxation time t. At 785 nm, the data points follow a single stretched-exponential function,

$$\alpha_{li}^{785}(I_p, t) = \alpha_{li}^{785}(I_p) \exp[-(t/\tau)^{\beta}], \quad (1)$$

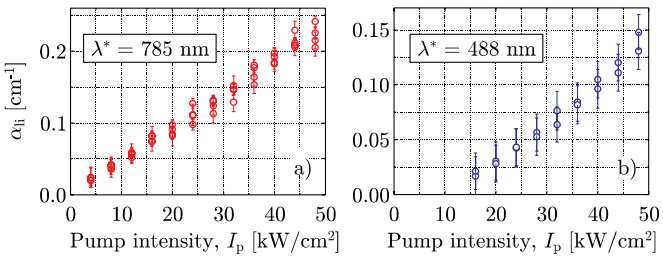

FIG. 2 (color online). The steady-state dependence $\alpha_{li}(I_p)$ at $\lambda^* = 785$ (a) and 488 nm (b). Four and two measurements at different sample positions are made in (a) and (b), respectively.

with the decay time $\tau \simeq 23.3$ ms and the stretching index $\beta \simeq 0.65$. At 488 nm, the data are well fitted by a superposition of two stretched-exponential functions with $\tau_{1,2} \simeq 6.1$ and 1.8 ms and $\beta_{1,2} \simeq 0.47$ and 1.67.

The stretched-exponential behavior found is typical for the LI absorption in lithium niobate [10,14,15]. It is commonly attributed to the relaxation of electrons from the intermediate Nb_{Li} levels near the CB to deeper centers. The difference between α_{li}^{785} and α_{li}^{488} is due to the fact that the cross section for the transitions $Nb_{Li} \rightarrow$ CB is maximum near 785 nm, $\sigma_{2c}^{785} \simeq 7 \times 10^{-18}$ cm^2 [9,16,17]. Holographic experiments with undoped lithium niobate at 532 nm show that the LI charge carriers are electrons [7]. Thus, different facts indicate that the observed LI absorption is due to population of the Nb_{Li} levels. The maximum concentration of electrons on these levels can be estimated from the data in Fig. 2(a) as $\alpha_{li}^{785}/\sigma_{2c}^{785} \simeq 3.3 \times 10^{16}$ cm^{-3}.

However, a serious problem arises when one tries to answer the following question: where do the photoactive electrons in the intermediate levels come from? They cannot be excited from remnant Fe-like deep traps: the remnant electron concentrations $\sim 10^{16}$ cm^{-3} are too high for undoped crystals, and they would lead to substantial initial light absorption. Also, they cannot be attributed to the two-photon absorption: this process is important at high pump intensities [14,15], $I_p \gg 1$ MW/cm^2, typical for pulse experiments, but it can be discarded in our case because the value of the two-photon absorption coefficient

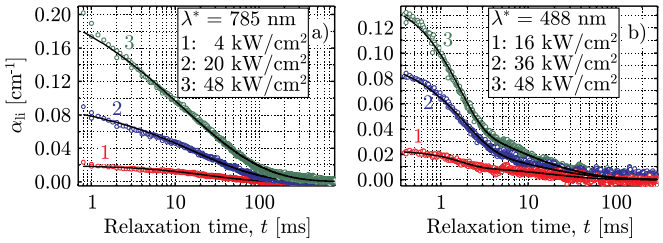

FIG. 3 (color online). The relaxation dependence $\alpha_{li}(t)$ (open circles) at $\lambda^* = 785$ (a) and 488 nm (b) for different pump intensities. The solid lines are stretched-exponential fits (see the text). Note a difference in the horizontal scales in (a) and (b).

is too small (smaller than 0.4 cm/GW) [18]. Furthermore, the dependence $\alpha_{li} \propto I_p^2$, being typical for two-photon absorption, is not the case in our experiments. Below, we propose a model to explain the new experimental results.

We assume, see Fig. 4, that in addition to the intermediate level 2 and deep level 1, an energy level 0—a hidden reservoir of electrons— occurs near the VB. The concentrations of the centers 0, 1, and 2 are $N_{0,1,2}$, and the corresponding electron concentrations are $n_{0,1,2}$. The VB is not supposed to be a source of electrons: vast experimental data show no sign of excitation of free and, hence, mobile holes in the visible cw range [6–10]; such an excitation occurs only in the UV range [13]. The direct excitation channel $0 \rightarrow$ CB is forbidden: the energy $\hbar\omega_p$ is insufficient for single-photon transitions. The direct recombination CB $\rightarrow 0$ is neglected: nonradiative processes are inefficient for large energy distances. The condition $N_1 \ll N_0 \lesssim N_2 \approx 10^{20}$ cm^{-3} provides a bottleneck for the excitation and recombination processes. We also assume that electrons excited to the CB drop quickly ($\lesssim 0.1$ ps) to the intermediate level 2 [16,19].

Within our model, the balance equations for $n_{0,2}$ are

$$\begin{aligned} \dot{n}_0 &= -q_{01} I_p n_0 (N_1 - n_1) + \gamma_{10} n_1 (N_0 - n_0), \\ \dot{n}_2 &= \nu_{1c} I_p n_1 - \gamma_{21} n_2 (N_1 - n_1); \end{aligned} \tag{2}$$

the dot indicates the time derivative, q_{01} and ν_{1c} are the excitation constants, and γ_{10} and γ_{21} are the recombination constants. Equations (2) are supplemented by the conservation law $n_0 + n_1 + n_2 = \bar{n}$, where $\bar{n} = \text{const}$ is the total concentration of photoactive electrons. It is useful to introduce the absorption cross sections σ_{01} and σ_{1c} and the relaxation times τ_{10} and τ_{21} according to

$$q_{01} N_1 = \frac{\sigma_{01}}{\hbar\omega_p}, \quad \nu_{1c} = \frac{\sigma_{1c}}{\hbar\omega_p}, \quad \gamma_{10} N_0 = \tau_{10}^{-1}, \quad \gamma_{21} N_1 = \tau_{21}^{-1}. \tag{3}$$

The values of σ_{1c} and τ_{21} can be deduced from the literature [6,8] and our experimental data, respectively. Two dimensionless parameters characterizing the impact of the zero centers, $a = N_1/N_0$ and $b = (\sigma_{01}\tau_{10}/\sigma_{1c}\tau_{21})^{1/2}$, will be of prime importance.

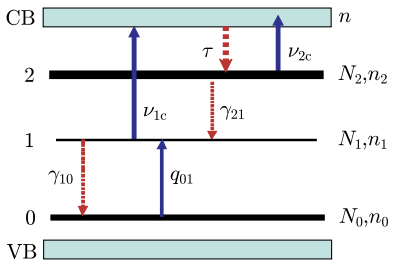

FIG. 4 (color online). Energy diagram for undoped crystals. The arrows indicate the excitation and recombination processes; the subscripts $1c$ and $2c$ indicate transitions $1 \rightarrow$ CB and $2 \rightarrow$ CB. The thicker the line, the larger is the corresponding quantity.

The next goal is to find the conditions for the quasilinear dependence $n_2(I_p)$ in the steady state and for domination of the absorption channel $2 \rightarrow$ CB, corresponding to excitations from the intermediate centers. Our analysis shows that for $a, b \ll 1$ and $I_p \ll I_p^{sat} \equiv \hbar\omega_p/\sqrt{\sigma_{01}\tau_{10}\sigma_{1c}\tau_{21}}$, the concentration n_2 is given by

$$n_2 \simeq 0.9 N_0 I_p / I_p^{sat}, \tag{4}$$

while $n_0 \approx N_0$. For $I_p \gtrsim I_p^{sat}$, the function $n_2(I_p)$ saturates, and the zero levels become exhausted.

Figure 5 illustrates our analysis. The solid line 1 is a superposition of four lines for $(a, b) = (0.001, 0.0001)$, $(0.001, 0.01)$, $(0.01, 0.01)$, and $(0.01, 0.001)$. Up to $I_p/I_p^{sat} \approx 0.3$, this line can be approximated by the linear function $0.9 I_p/I_p^{sat}$ with a 5% accuracy. Deviations from the linear dependence, which occur for $I_p/I_p^{sat} \lesssim 10^{-2}$, are invisible in the scale used; the smaller a and b, the weaker are these deviations. Increasing a results eventually in strong deviations from the quasilinear dependence (see curves 2–4). Variation of the total electron concentration $\bar{n}$ between N_0 and $N_0 + N_1$, i.e., variation of $n_1(I_p = 0)$ between 0 and N_1, does not really affect the described behavior. Interestingly, the model also predicts the shifted linear dependence $n_2 \propto \alpha_{li} \propto c_1 I_p - c_2$, similar to that of Fig. 2(b), in the intermediate range of I_p (see curves 2 and 3 in Fig. 5).

Let us adapt the model to the experimental data of Fig. 2(a) for $\lambda^* = 785$ nm. The contribution to α_{li} from the transition $2 \rightarrow$ CB is $\alpha_{2c} = \sigma_{2c}^* n_2$. Using Eq. (4) and the definition of I_p^{sat}, we can express the slope as

$$\frac{d\alpha_{2c}}{dI_p} \simeq \frac{0.9\sigma_{2c}^* N_0}{\hbar\omega_p} \sqrt{\sigma_{01}\tau_{10}\sigma_{1c}\tau_{21}}. \tag{5}$$

Setting $\sigma_{1c} = 4 \times 10^{-18}$ cm^2 [6], $\sigma_{2c}^* = 6 \times 10^{-18}$ cm^2 [16,17], and $\tau_{21} = 20$ ms (in accordance with the

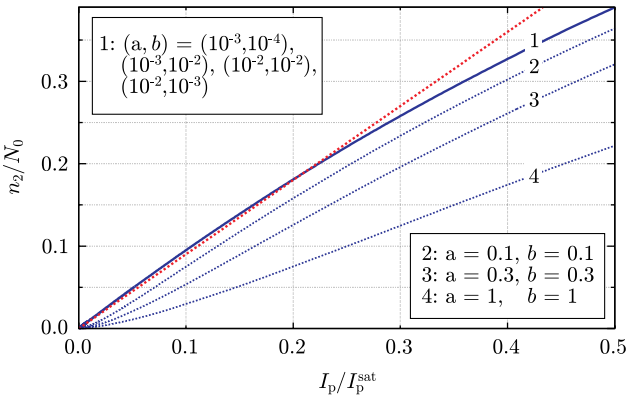

FIG. 5 (color online). Curves 1 to 4: steady-state dependence $n_2(I_p)$ calculated from Eqs. (2) for different pairs (a, b) and $\bar{n} = N_0$. The straight dotted line is $0.9 I_p/I_p^{sat}$.

experiment), we estimate $N_0(\sigma_{01}\tau_{10})^{1/2} \approx 10^3\ \mathrm{s}^{1/2}\,\mathrm{cm}^{-2}$. Also, we must fulfill the condition $I_p^{sat} \gtrsim 10^5\ \mathrm{W/cm}^2$, which ensures the quasilinearity of $\alpha_{2c}(I_p)$ up to $\approx 50\ \mathrm{kW/cm}^2$. This gives the restriction $\sigma_{01}\tau_{10} \lesssim 10^{-28}\ \mathrm{cm}^2\,\mathrm{s}$ and, correspondingly, the inequalities $b \lesssim 10^{-4}$ and $N_0 \gtrsim 10^{17}\ \mathrm{cm}^{-3}$. They are in perfect agreement with the model assumptions. The second inequality restricts from below the concentration N_0: it must be at least 2 orders of magnitude larger than $N_1 \sim 10^{15}\ \mathrm{cm}^{-3}$.

Let us verify whether the other contributions to α_{li} are small. The contribution α_{1c}, i.e., absorption by center 1, can be estimated as $\alpha_{1c} \lesssim \sigma_{1c}^* N_0(\sigma_{01}\tau_{10}/\sigma_{1c}\tau_{21})^{1/2}$. Using the above numerical values, one can check that it is smaller than $10^{-5}\ \mathrm{cm}^{-1}$, i.e., negligible. The contribution $\alpha_{01} = \sigma_{01}^* n_0 \simeq \sigma_{01}^* N_0$ can be negligible only because σ_{01} is small. The sufficient restriction, $\sigma_{01} \lesssim 10^{-21}\ \mathrm{cm}^2$, is not severe for undoped crystals.

We claim that there is no contradiction between our model and the conventional description of experimental data for $LiNbO_3$ crystals doped with Fe or Cu, which does not include the zero centers. Two differences between doped and undoped $LiNbO_3$ crystals are important. (1) In doped crystals, the concentration N_1 is not small, and the contribution $\alpha_{1c} = \sigma_{1c} n_1$ is substantial in the low-intensity region. The contribution α_{01} can easily be negligible here owing to the smallness of σ_{01}. (2) Because of the localized nature of the centers 0 and 1, the product $\sigma_{01}\tau_{10}$ can be strongly different for doped and undoped crystals. This issue requires further study.

One might think that playing with numerous model parameters allows us to fit any particular measured dependence, but the actual situation is different. Characteristics of many processes involved in LI charge transport in lithium niobate are known, and hence, the remaining degrees of freedom are very limited. The explanation of the challenging experimental dependences has occurred within a narrow window of possible noncontradicting, state-of-the-art studies of lithium niobate.

Revision of the concept of the LI charge transport in $LiNbO_3$ crystals on the basis of new experimental facts is the main achievement of this study. The sources of photoactive electrons are not restricted to deep traps near the center of the band gap even at modest cw intensities. Numerous and much deeper centers, attributed to energy levels nearby the VB, are now expected to be important.

The presence of tails of the density of electronic states near the CB and VB is a general feature of partially disordered materials, including lithium niobate [20]. While the importance of the intermediate levels near the CB, attributed to the Nb_{Li} defects, is well recognized for $LiNbO_3$ crystals, the energy levels near the VB are only scarcely mentioned in the literature (as oxygen vacancies) with regard to the LI charge transport [8,14]. It is straightforward to expect that they are as important as the levels near the CB.

The question about the sources of photoactive electrons in $LiNbO_3$ crystals has important implications. If the sources are restricted to dopant-related levels, they can be emptied by thermal or optical treatments leading to suppression of optical damage [21,22]. If numerous deeper levels are involved in the charge transport at low or modest intensities, then additional efforts—like special doping—must be undertaken to remove them. The zero levels can possibly be emptied by oxidation of the crystals. Or lithium indiffusion may improve the stoichiometry of lithium niobate and diminish the impact of intrinsic defects.

In conclusion, we have presented novel experimental results showing a substantial linear light-induced absorption in undoped lithium niobate in the range of cw intensities, which contradicts the present notion of charge transport in this important optical material. A quantitative model involving energy levels near the valence band edge as a hidden reservoir of electrons is proposed, which explains the experimental features and essentially modifies the concept of light-induced charge transport.

Financial support of the Deutsche Forschungsgemeinschaft is gratefully acknowledged.

*luedtke@physik.uni-bonn.de

[1] L. Arizmendi, Phys. Status Solidi A **201**, 253 (2004).
[2] M. M. Fejer, G. A. Magel, D. H. Jundt, and R. L. Byer, IEEE J. Quantum Electron. **28**, 2631 (1992).
[3] V. S. Ilchenko, A. A. Savchenkov, A. B. Matsko, and L. Maleki, Phys. Rev. Lett. **92**, 043903 (2004).
[4] A. M. Glass, D. von der Linde, and T. J. Negran, Appl. Phys. Lett. **25**, 233 (1974).
[5] V. Fridkin and B. Sturman, *The Photovoltaic and Photorefractive Effects in Noncentrosymmetric Materials* (Gordon and Breach, New York, 1992).
[6] K. Buse, J. Imbrock, E. Krätzig, and K. Peithmann, in *Photorefractive Materials and Their Applications 2*, edited by P. Günter and J.-P. Huignard (Springer, New York, 2007), Chap. 4.
[7] F. Lüdtke, N. Waasem, K. Buse, and B. Sturman, Appl. Phys. B **105**, 35 (2011).
[8] E. Krätzig and O. F. Schirmer, in *Photorefractive Materials and Their Applications 2*, edited by P. Günter and J.-P. Huignard (Springer, New York, 1989), Chap. 5.
[9] F. Jermann and J. Otten, J. Opt. Soc. Am. B **10**, 2085 (1993).
[10] D. Berben, K. Buse, S. Wevering, P. Herth, M. Imlau, and Th. Woike, J. Appl. Phys. **87**, 1034 (2000).
[11] M. Carrascosa, J. Villaroel, J. Carnicero, A. García-Cabañes, and J. M. Cabrera, Opt. Express **16**, 115 (2008).
[12] B. Sturman, M. Carrascosa, and F. Agulló-López, Phys. Rev. B **78**, 245114 (2008).
[13] R. Orlowski and E. Krätzig, Solid State Commun. **27**, 1351 (1978).
[14] P. Herth, T. Granzow, D. Schaniel, Th. Woike, M. Imlau, and E. Krätzig, Phys. Rev. Lett. **95**, 067404 (2005).
[15] C. Merschjann, B. Schoke, and M. Imlau, Phys. Rev. B **76**, 085114 (2007).

[16] O. Beyer, D. Maxein, K. Buse, B. Sturman, H. T. Hsieh, and D. Psaltis, Phys. Rev. E **71**, 056603 (2005).
[17] C. Merschjann, B. Schoke, D. Conradi, M. Imlau, G. Corradi, and K. Polgár, J. Phys. Condens. Matter **21**, 015906 (2009).
[18] R. DeSalvo, A. Said, D. Hagan, E. Van Stryland, and M. Sheik-Bahae, IEEE J. Quantum Electron. **32**, 1324 (1996).
[19] P. Reckenthaeler, D. Maxein, Th. Woike, K. Buse, and B. Sturman, Phys. Rev. B **76**, 195117 (2007).
[20] N. F. Mott and E. A. Davis, *Electron Processes in Non-Crystalline Materials* (Clarendon, Oxford, 1979).
[21] M. Kösters, B. Sturman, P. Werheit, D. Haertle, and K. Buse, Nature Photon. **3**, 510 (2009).
[22] M. Falk and K. Buse, Appl. Phys. B **81**, 853 (2005).